Analysis of Landau–Lifshitz and neo-Hookean models for static and dynamic acoustoelastic testing

Physica Scripta

PAPER

Analysis of Landau–Lifshitz and neo-Hookean models for static and dynamic acoustoelastic testing

Andrey Melnikov[1], **Alison E Malcolm**[2,*] **and Kristin M Poduska**[3]

[1] Department of Mathematics, Nazarbayev University, Astana, 010000, Kazakhstan
[2] Department of Earth Sciences, Memorial University, St. John's, NL, A1B 3X5, Canada
[3] Department of Physics and Physical Oceanography, Memorial University, St. John's, NL, A1B 3X7, Canada
[*] Author to whom any correspondence should be addressed.

E-mail: andrey.melnikov@nu.edu.kz, amalcolm@mun.ca and kris@mun.ca

Keywords: continuum mechanics, acoustoelasticity, mechanical waves

OPEN ACCESS

RECEIVED
9 July 2022

REVISED
1 October 2022

ACCEPTED FOR PUBLICATION
18 October 2022

PUBLISHED
16 November 2022

Abstract

A comparison of three different isotropic non-linear elastic models uncovers subtle but important differences in the acoustoelastic responses of a material slab that is subjected to dynamic deformations during a pump-probe experiment. The probe wave deformations are small and are superimposed on larger underlying deformations using three different models: Landau–Lifshitz (using its fourth-order extension), compressible neo-Hookean model (properly accounting for volumetric deformations), and an alternative neo-Hookean model (fully decoupled energies due to distortional isochoric and volumetric deformations). The analyses yield elasticity tensors and respective expressions for the propagation speeds of P-wave and S-wave probes for each model. Despite having many similarities, the different models give different predictions of which probe wave types will have speeds that are perturbed by different pump wave types. The analyses also show a conceptual inconsistency in the Landau–Lifshitz model, that a simple shear deformation induces a stress and a shear wave probe speed that depend on the second-order elastic constant λ, which controls resistance to volumetric changes and thus should not be present in the expressions for shear stress and shear wave probe speeds. Thus, even though the Landau–Lifshitz model is widely used, it may not always be the best option to model experimental data.

1. Introduction

Understanding non-linear acoustoelastic wave propagation in solids is important for non-destructive testing applications [1–4]. All acoustoelastic techniques are based on the fact that propagating wave speeds vary with deformation or applied stress, whether those stresses are static or dynamic. While the experimental principles of static acoustoelasticity are considered to be well-established [5], the consistency of some theoretical results [6, 7] has been questioned [5].

Thus, the theoretical underpinnings of dynamic acoustoelasticity and associated experimental conditions require more understanding. The present work compares several different theoretical models that are relevant to experimental investigations of static and dynamic acoustoelasticity.

Dynamic acoustoelastic testing [8–10] is gaining popularity for characterizing the structure of complex solids such as bones [11], rocks [8, 12] and other materials [9]. In such experiments, a large amplitude (pump) wave provides a dynamic deformation field, which perturbs the speed of a second (probe) wave. The probe wave amplitude is sufficiently small that its influence on the pump-induced deformation can be neglected. One appeal of the pump-probe approach is that it can be applied under field conditions using artificial sources and receivers [13]. Although the pump-induced deformation fields used in dynamic acoustoelastic testing are typically smaller than static deformations induced by mechanical presses (for example), nonlinear wave effects in rocks can be observed at strains as low as 10^{-8}, and thus dynamic acoustoelastic testing is feasible even with small strains [14]. Furthermore, this sort of testing can be performed in the presence of both a static deformation (due to an applied load) and a pump-induced dynamic deformation [15], as shown in figure 1.

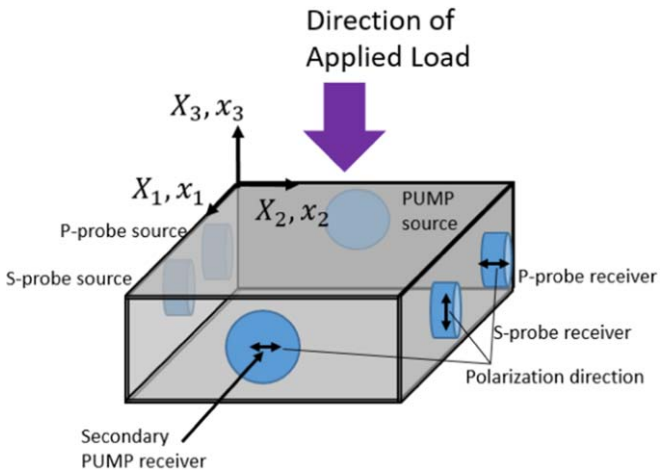

Figure 1. A schematic diagram of a dynamic acoustoelastic pump-probe experiment. The pump source generates a dynamic deformation field that perturbs the speed of the probe wave (produced by the source and detected at the receiver). An optional static deformation can be induced by an applied load. The pump and probe source waves can have either P or S polarizations. The upper-case (X_i) and lower-case (x_i) coordinate systems correspond to the reference and current configurations of the sample, respectively.

The primary challenge with modelling static and dynamic acoustoelasticity is that, in order to apply the theory in a tractable manner, we must make assumptions about the nature of the material as well as the nature of the waves.

To provide a better foundation for applying theoretical models to dynamic acoustoelastic experiments, this paper outlines three different isotropic models and their assumptions. The emphasis is on demonstrating that, even in an isotropic material, pump waves can perturb the wave speeds of sensing probe waves in qualitatively different ways, depending on the choice of model. After giving continuum mechanics definitions related to deformations (section 2), section 3 summarizes results for strain-energy functions of a variable-order model (Landau–Lifshitz in its fourth-order extension), as well as two different compressible neo-Hookean models. Then, section 4 presents general wave speed expressions for probe waves (P- and S-wave) for each model, and section 5 considers their application to an experimental scenario with both static and dynamic predeformations. Section 6 discusses the obtained theoretical results, and gives additional explanations in the context of non-linear elasticity. Short conclusions are given in section 7.

2. Basic continuum mechanics: deformations

For all three elastic models described herein, the basic aspects of continuum mechanics apply. In particular, the focus is on how a deformation changes a material from its reference configuration to a current configuration. A schematic representation of one such material is shown in figure 1.

A material point in the reference configuration $\mathscr{B}_\mathrm{r}$ is labelled by a position vector $\mathbf{X}$, and this point in the current configuration $\mathscr{B}$ at time t is labelled by a position vector $\mathbf{x}$. Deformation is described by the vector field $\boldsymbol{\chi}$, which relates the position of a particle in the reference configuration to the position of the same particle in the current configuration: $\mathbf{x} = \boldsymbol{\chi}(\mathbf{X}, t)$. The deformation gradient tensor, denoted $\mathbf{F}$, is defined by

$$\mathbf{F} = \mathrm{Grad}\boldsymbol{\chi},$$

where Grad is the gradient operator defined with respect to $\mathbf{X}$. The left and right Cauchy-Green deformation tensors are related to the deformation gradient and defined by

$$\mathbf{B} = \mathbf{F}\mathbf{F}^\mathrm{T}, \quad \text{and } \mathbf{C} = \mathbf{F}^\mathrm{T}\mathbf{F}, \tag{1}$$

respectively. Volumetric deformation is accounted for by

$$J = \det\mathbf{F}. \tag{2}$$

In the absence of deformation in the reference configuration and for the isochoric, volume preserving deformation (2) reduces to $J = 1$. The Green (Lagrangian) strain tensor can be obtained from

$$\mathbf{E} = \frac{1}{2}(\mathbf{F}^\mathrm{T}\mathbf{F} - \mathbf{I}). \tag{3}$$

3. Isotropic non-linear elastic models

While for the linear isotropic material there is only one universal model (all materials are treated as Hookean solids in linear elasticity), the situation in nonlinear elasticity is much more complicated and there are different models even for isotropic (nonlinear) materials. Thus, it is impossible to indicate a general universal model in nonlinear elasticity suitable for all cases. One of the aims of this paper is to shed light on the differences of different nonlinear elastic models specifically within the context of acoustoelasticity.

Many different non-linear elastic models exist, including neo-Hookean [16], Mooney-Rivlin [17], Gent [18], Arruda-Boyce [19], Blatz-Ko and Ogden models [20], and Landau–Lifshitz [21, 22]. The Landau–Lifshitz (L-L) is a third-order model that is frequently used in acoustoelastic applications because it can accommodate different orders of non-linearity (by expanding it to the next order). However, this model has a large number of fitable parameters, some of which have unclear physical meanings. Furthermore, the L-L model does not provide a clear way of capturing volumetric deformations. Other models, such as neo-Hookean models, are better suited to deal with both distortional and dilatational deformations. In a modified neo-Hookean model, it is also feasible to decouple energies due to distortional isochoric and volumetric deformations. The following subsections describe each of these three models in more detail.

3.1. Landau–Lifshitz model: adjustable order of non-linearity

The L-L model was initially proposed as a third-order expansion of the strain-energy function, W, in terms of the Green strain tensor $\mathbf{E}$. It appears that formulas for wave speeds as a function of strain, relevant for the fourth-order model have not been derived in the literature in a general form. Therefore, we first recall the fourth-order expansion of this model.

The fourth-order expansion of the L-L elasticity model is built from a third-order expansion of the strain energy function[4], which gives us

$$W(I_1, I_2, I_3) = \frac{\lambda}{2}I_1^2 + \mu I_2 + \frac{A}{3}I_3 + BI_1I_2 + \frac{C}{3}I_1^3 + EI_1I_3 + FI_1^2I_2 + GI_2^2 + HI_1^4, \tag{4}$$

where invariants

$$I_1 = \mathrm{tr}\mathbf{E}, \quad I_2 = \mathrm{tr}\mathbf{E}^2, \quad I_3 = \mathrm{tr}\mathbf{E}^3,$$

λ and μ are second-order elastic constants (Lamé's parameters), A, B, C are the third-order elastic constants, and E, F, G, H are the fourth-order elastic constants. Thus, this model allows for a choice of non-linearity order. For example, dropping fourth-order terms in (4) leads to a third-order strain-energy function, and to a second-order stress-strain relation, since taking a derivative reduces the order of nonlinearity by one.

Since the strain-energy function (4) depends on the Green strain tensor $\mathbf{E}$, it is convenient to work with the second Piola-Kirchhoff stress tensor, $\mathbf{S}$, which is a derivative of strain-energy W with respect to $\mathbf{E}$. Since (4) depends on $\mathbf{E}$ through invariants I_1, I_2, I_3, we use a chain rule to obtain second Piola-Kirchhoff stress tensor as

$$\mathbf{S} = \frac{\partial W}{\partial \mathbf{E}} = \frac{\partial W}{\partial I_1}\frac{\partial I_1}{\partial \mathbf{E}} + \frac{\partial W}{\partial I_2}\frac{\partial I_2}{\partial \mathbf{E}} + \frac{\partial W}{\partial I_3}\frac{\partial I_3}{\partial \mathbf{E}}. \tag{5}$$

We calculate the required derivatives of the invariants

$$\frac{\partial I_1}{\partial \mathbf{E}} = \mathbf{I}, \quad \frac{\partial I_2}{\partial \mathbf{E}} = 2\mathbf{E}, \quad \frac{\partial I_3}{\partial \mathbf{E}} = 3\mathbf{E}^2, \tag{6}$$

where $\mathbf{I}$ is the identity tensor. From the strain energy function (4), we also obtain

$$\frac{\partial W}{\partial I_1} = \lambda I_1 + BI_2 + CI_1^2 + EI_3 + 2FI_1I_2 + 4HI_1^3, \tag{7}$$

$$\frac{\partial W}{\partial I_2} = \mu + BI_1 + FI_1^2 + 2GI_2, \tag{8}$$

$$\frac{\partial W}{\partial I_3} = A/3 + EI_1. \tag{9}$$

[4] The derivation is based on Taylor series expansion formula for the function of three variables $W(I_1, I_2, I_3)$ near the point of zero strain.

Substituting the previous expressions (6), (7), (8), (9) into (5), we obtain a general expression for stress

$$\mathbf{S} = \frac{\partial W}{\partial \mathbf{E}} = (\lambda I_1 + BI_2 + CI_1^2 + EI_3 + 2FI_1I_2 + 4HI_1^3)\mathbf{I} + 2(\mu + BI_1 + FI_1^2 + 2GI_2)\mathbf{E} + (A + 3EI_1)\mathbf{E}^2. \tag{10}$$

3.2. Neo-Hookean model 1: volumetric deformations

The L-L model and its fourth-order extension is frequently used in acoustoelastic applications, but there is no clear term in expression (4) that specifically pertains to volume deformations. A simple calculation (given in appendix A) for simple shear leads to an expression in stress components containing Lamé's parameter λ, which measures the resistance to volume deformation. This is problematic because simple shear does not induce a volumetric deformation. To mitigate these limitations, we consider a compressible neo-Hookean model, where volumetric deformations are clearly captured by changes in the determinant of the right Cauchy-Green deformation tensor.

A compressible neo-Hookean model can take the form [23]

$$W = \frac{\mu}{2}(I_1 - 3) - \mu \ln \sqrt{I_3} + \frac{\lambda}{2}(\ln \sqrt{I_3})^2, \tag{11}$$

where λ and μ are Lamé's parameters in the reference configuration and we use another set of invariants of the right Cauchy-Green deformation tensor $(1)_2$.

The stress can be expressed in terms of first Piola-Kirchhoff stress tensor, from the derivative of the strain-energy function with respect to the deformation gradient tensor

$$\mathbf{P} = \frac{\partial}{\partial \mathbf{F}}(W(I_1, I_2, I_3)),$$

where the strain-energy is defined in terms of invariants used for isotropic materials

$$I_1 = \mathrm{tr}\mathbf{C}, \quad I_2 = \frac{1}{2}\{(\mathrm{tr}\mathbf{C})^2 - \mathrm{tr}\mathbf{C}^2\}, \quad I_3 = \det\mathbf{C}.$$

The choice of first the Piola-Kirchhoff stress is convenient here because the strain-energy function (11) depends on $\mathbf{C}$, and $\mathbf{C} = F^{\mathrm{T}}F$.

Using a chain rule and the following relations

$$\frac{\partial I_1}{\partial \mathbf{F}} = 2\mathbf{F}, \quad \frac{\partial I_2}{\partial \mathbf{F}} = 2I_1\mathbf{F} - 2\mathbf{F}\mathbf{F}^{\mathrm{T}}\mathbf{F}, \quad \frac{\partial I_3}{\partial \mathbf{F}} = 2I_3\mathbf{F}^{-\mathrm{T}},$$

we obtain

$$\mathbf{P} = 2W_1\mathbf{F} + 2W_2(I_1\mathbf{F} - \mathbf{F}\mathbf{F}^{\mathrm{T}}\mathbf{F}) + 2W_3I_3\mathbf{F}^{-\mathrm{T}}, \tag{12}$$

where W_1, W_2, W_3 are partial derivatives of W with respect to I_1, I_2, I_3, respectively.

For completeness, the expression for Cauchy stress $\boldsymbol{\sigma}$ can be found using a standard relation

$$J\boldsymbol{\sigma} = \mathbf{P}\mathbf{F}^{\mathrm{T}} = 2W_1\mathbf{B} + 2W_2(I_1\mathbf{I} - \mathbf{B})\mathbf{B} + 2W_3I_3\mathbf{I},$$

where $\mathbf{B} = \mathbf{F}\mathbf{F}^{\mathrm{T}}$ is the left Cauchy-Green deformation tensor and $J = \det\mathbf{F}$.

Specifically, for the strain energy (11) we obtain

$$J\boldsymbol{\sigma} = \mu\mathbf{B} + (\lambda \ln \sqrt{I_3} - \mu)\mathbf{I}. \tag{13}$$

3.3. Neo-Hookean model 2: fully decoupled energies due to distortional isochoric and volumetric deformations

In neo-Hookean model 1 (11), the first term is sensitive to both distortional and dilatational deformations. It will be shown that decoupling energies has an effect on the action of P- and S-waves (pumps) on probes. We recall that P- and S-wave pumps are related to dilatational/compressional and shear (distortional) deformations, respectively.

To this end, consider the strain-energy function

$$W = \frac{\mu}{2}(\bar{I}_1 - 3) + \frac{k}{2}(J - 1)^2, \tag{14}$$

where $\bar{I}_1 = \mathrm{tr}\bar{\mathbf{C}}$ and k is the bulk modulus. The first term is only sensitive to distortional, isochoric deformations and the second term is sensitive to volumetric deformations.

Any deformation gradient can be decomposed into

$$\mathbf{F} = J^{\frac{1}{3}}\bar{\mathbf{F}},$$

where $\bar{\mathbf{F}}$ is a distortional part of the deformation gradient [23]. Accordingly, in terms of the right Cauchy-Green deformation tensor,

$$\bar{\mathbf{C}} = I_3^{-\frac{1}{3}}\mathbf{C}.$$

Therefore, the invariant $\bar{I}_1$ accounting for pure distortional deformation is

$$\bar{I}_1 = \mathrm{tr}\bar{\mathbf{C}} = \mathrm{tr}(I_3^{-\frac{1}{3}}\mathbf{C}) = I_3^{-\frac{1}{3}}\mathrm{tr}\mathbf{C} = I_3^{-\frac{1}{3}}I_1.$$

The first Piola-Kirchhoff stress tensor can be obtained from (14) after some rearrangements

$$\mathbf{P} = \mu I_3^{-1/3}\left(-\frac{1}{3}I_1\mathbf{F}^{-\mathrm{T}} + \mathbf{F}\right) + k(I_3 - \sqrt{I_3})\mathbf{F}^{-\mathrm{T}}. \tag{15}$$

4. Wave speeds in different models

Since dynamic acoustoelasticity experiments interpret wave speed changes (inferred from changes in traveltimes), this section derives wave speed expressions from each of the three models by using the theory of infinitesimal deformations [24] (such as small amplitude probe waves), superimposed on large deformations (such as large amplitude pump waves or static deformation induced by a press machine).

4.1. Equation of motion, elasticity and acoustic tensors

Consider an incremental equation of motion [24] (Ch. 6)

$$\mathrm{div}\dot{\mathbf{T}}_0 = \rho\frac{\partial^2\mathbf{u}}{\partial t^2}, \tag{16}$$

where $\dot{\mathbf{T}}_0$ is the increment in the nominal stress tensor corresponding to the displacement $\mathbf{u}$, caused by the probe wave, and ρ is a mass density in the current configuration. The nominal stress tensor is a transpose of first Piola-Kirchhoff stress tensor.

An increment in the nominal stress tensor is given by the constitutive law

$$\dot{T}_{0pi} = \mathscr{A}_{0piqj}u_{j,q}, \tag{17}$$

where $\mathcal{A}_0$ is the fourth-order elasticity tensor (defined in component form by expression (24)).

Substituting (17) in (16), we obtain

$$(\mathcal{A}_{0piqj}u_{j,q})_{,p} = \rho\frac{\partial^2 u_i}{\partial t^2}. \tag{18}$$

The small amplitude probe wave propagates within a small area of the sample and we assume that in this area deformation is essentially homogeneous and static due to the low-frequency pump wave. Basically, we assume that changes in the deformation are so small that they can be neglected (during a short time window required for the probe to travel across the sample). Therefore, equation (18) can be rewritten

$$\mathcal{A}_{0piqj}u_{j,qp} = \rho\frac{\partial^2 u_i}{\partial t^2}. \tag{19}$$

In general, the probe wave displacement can be written

$$\mathbf{u} = \mathbf{m}f(\mathbf{n}\cdot\mathbf{x} - vt),$$

where f is a twice differentiable function, unit vector $\mathbf{m}$ represents polarization direction, unit vector $\mathbf{n}$ gives propagation direction, and v is the propagation speed of a probe wave. We then obtain

$$\frac{\partial^2 u_j}{\partial x_q \partial x_p} = m_j f''(\mathbf{n}\cdot\mathbf{x} - vt)n_q n_p, \tag{20}$$

and

$$\frac{\partial^2 u_i}{\partial t^2} = m_i f''(\mathbf{n}\cdot\mathbf{x} - vt)v^2. \tag{21}$$

Substituting these into (19) and multiplying both sides of (19) by $J = \rho_0/\rho$, where ρ_0 is a mass density in the reference configuration, we obtain

$$J\mathcal{A}_{0piqj}n_p n_q m_j = \rho_0 v^2 m_i, \tag{22}$$

which is analogous to the Christoffel equations but for non-linear elastic case. More compactly, we can rewrite (22) as

$$\mathbf{Q}(\mathbf{n})\mathbf{m} = \rho_0 v^2 \mathbf{m}, \tag{23}$$

where $Q_{ij}(\mathbf{n}) = J\mathcal{A}_{0piqj}n_p n_q$ is the acoustic tensor. Finally, in the current configuration, elastic tensor moduli can be obtained for the compressible case [25]

$$J\mathcal{A}_{0jilk} = F_{j\alpha}F_{l\beta}\frac{\partial^2 W}{\partial F_{i\alpha}\partial F_{k\beta}}. \tag{24}$$

Based on these tensor expressions, we now consider each of our three models separately, and substitute the specific forms of strain energy W into equation (24). From this, we derive expressions for how a pump wave (that causes changes in W) affects the velocity of a probe wave (via changes in the velocities determined by the moduli in the LHS of (24)). A summary of results from all possible probe-pump combinations is shown in table 1.

4.2. Wave speeds: L-L model

We substitute strain-energy function (4) into (24). The details of this calculation leading to expression (25) are given in appendix B. After some lengthy rearrangements, we obtain

$$\begin{aligned} J\mathcal{A}_{0jilk} = {} & (\lambda + 2CI_1 + 2FI_2 + 12HI_1^2)B_{ji}B_{lk} \\ & + (2B + 3E + 4FI_1)B_{ji}M_{lk} \\ & + (2B + 4FI_1 + 3E)B_{lk}M_{ji} + 8GM_{ji}M_{kl} \\ & + (\mu + BI_1 + FI_1^2 + 2GI_2)(B_{jk}B_{li} + B_{jl}B_{ki}) \\ & + (A + 3AI_1)(B_{jk}M_{li} + B_{li}M_{jk}) \\ & + B_{jl}\delta_{ik}(\lambda I_1 + BI_2 + CI_1^2 + EI_3 + 2FI_1I_2 + 4HI_1^3) \\ & + 2M_{jl}\delta_{ik}(\mu + BI_1 + FI_1^2 + 2GI_2) + \bar{M}_{jl}\delta_{ik}, \end{aligned} \tag{25}$$

where $\mathbf{B} = \mathbf{F}\mathbf{F}^{\mathrm{T}}$ is the left Cauchy-Green deformation tensor. Also, in (25) we have introduced two new quantities: Eulerian symmetric tensors $\mathbf{M} = \mathbf{F}\mathbf{E}\mathbf{F}^{\mathrm{T}}$ and $\bar{\mathbf{M}} = \mathbf{F}\mathbf{E}^2\mathbf{F}^{\mathrm{T}}$. Note that expression (25), as expected, is consistent with linear elastic theory. In the reference configuration, where $J = 1, I_1 = I_2 = I_3 = 0, \mathbf{B} = I$, $\mathbf{M} = \bar{M} = 0$, we recover the classical expression $\mathcal{A}_{0jilk} = \lambda\delta_{ji}\delta_{lk} + \mu(\delta_{jk}\delta_{li} + \delta_{jl}\delta_{ki})$.

In total, there are 9 expressions for probe wave speeds[5], and each expression would be evaluated for 10 cases of deformation caused by a pump wave. We show the result for a P-wave probe propagating in the X_1 direction and S-wave probe propagating in X_1 direction and polarized in X_3 direction for *any* underlying deformation. This accommodates any kind of underlying deformation, whether static deformations or pump waves, since such deformations manifest in the following equations via tensors $\mathbf{B}, \mathbf{M}, \bar{\mathbf{M}}$, and the invariants I_1, I_2, I_3.

For this example case, the P-wave probe speed from (23) and (25) is

$$\begin{aligned} \rho_0 v_{11}^2 = J\mathcal{A}_{01111} = {} & (\lambda + 2CI_1 + 2FI_2 + 12HI_1^2)B_{11}B_{11} \\ & + (2B + 3E + 4FI_1)B_{11}M_{11} \\ & + (2B + 4FI_1 + 3E)B_{11}M_{11} + 8GM_{11}M_{11} \\ & + 2(\mu + BI_1 + FI_1^2 + 2GI_2)B_{11}B_{11} \\ & + 2(A + 3AI_1)B_{11}M_{11} \\ & + B_{11}(\lambda I_1 + BI_2 + CI_1^2 + EI_3 + 2FI_1I_2 + 4HI_1^3) \\ & + 2M_{11}(\mu + BI_1 + FI_1^2 + 2GI_2) + \bar{M}_{11}. \end{aligned} \tag{26}$$

and the S-wave probe speed is

$$\begin{aligned} \rho_0 v_{31}^2 = J\mathcal{A}_{01313} = {} & (\lambda + 2CI_1 + 2FI_2 + 12HI_1^2)B_{13}B_{13} \\ & + (2B + 3E + 4FI_1)B_{13}M_{13} \\ & + (2B + 4FI_1 + 3E)B_{13}M_{13} + 8GM_{13}M_{31} \\ & + (\mu + BI_1 + FI_1^2 + 2GI_2)(B_{13}B_{13} + B_{11}B_{33}) \\ & + 2(A + 3AI_1)B_{13}M_{13} \\ & + B_{11}(\lambda I_1 + BI_2 + CI_1^2 + EI_3 + 2FI_1I_2 + 4HI_1^3) \\ & + 2M_{11}(\mu + BI_1 + FI_1^2 + 2GI_2) + \bar{M}_{11}, \end{aligned} \tag{27}$$

[5] More precisely, these are speeds v_{ij}, where $i \in \{1, 2, 3\}, j \in \{1, 2, 3\}$; indices i and j correspond to the direction of polarization and direction of propagation of a wave, respectively.

Table 1. Summary of probe wave types whose speeds are perturbed by each pump wave type. ✓ indicates a perturbation; X indicates no perturbation; X^* indicates a weak perturbation due to deformation in an unconstrained direction. In speed v_{ij}, i denotes polarization direction and j indicates propagation direction.

L-L model (4)

probe	P-wave pump				S-wave pump					
	P_{11}	P_{22}	P_{33}	Spher. P	S_{12}	S_{13}	S_{21}	S_{23}	S_{32}	S_{31}
p_{11}	✓	✓	✓	✓	✓	✓	✓	✓	✓	✓
p_{22}	✓	✓	✓	✓	✓	✓	✓	✓	✓	✓
p_{33}	✓	✓	✓	✓	✓	✓	✓	✓	✓	✓
s_{31}	✓	✓	✓	✓	✓	✓	✓	✓	✓	✓
s_{21}	✓	✓	✓	✓	✓	✓	✓	✓	✓	✓
s_{12}	✓	✓	✓	✓	✓	✓	✓	✓	✓	✓
s_{32}	✓	✓	✓	✓	✓	✓	✓	✓	✓	✓
s_{23}	✓	✓	✓	✓	✓	✓	✓	✓	✓	✓
s_{13}	✓	✓	✓	✓	✓	✓	✓	✓	✓	✓

Neo-Hookean model 1 (11)

probe	P-wave pump				S-wave pump					
	P_{11}	P_{22}	P_{33}	Spher. P	S_{12}	S_{13}	S_{21}	S_{23}	S_{32}	S_{31}
p_{11}	✓	✓	✓	✓	✓	✓	×	×	×	×
p_{22}	✓	✓	✓	✓	×	×	✓	✓	×	×
p_{33}	✓	✓	✓	✓	×	×	×	×	✓	✓
s_{31}	✓	$\times^*$	$\times^*$	✓	✓	✓	×	×	×	×
s_{21}	✓	$\times^*$	$\times^*$	✓	✓	✓	×	×	×	×
s_{12}	$\times^*$	✓	$\times^*$	✓	×	×	✓	✓	×	×
s_{32}	$\times^*$	✓	$\times^*$	✓	×	×	✓	✓	×	×
s_{23}	$\times^*$	$\times^*$	✓	✓	×	×	×	×	✓	✓
s_{13}	$\times^*$	$\times^*$	✓	✓	×	×	×	×	✓	✓

Neo-Hookean model 2 (decoupled energies) (14)

probe	P-wave pump				S-wave pump					
	P_{11}	P_{22}	P_{33}	Spher. P	S_{12}	S_{13}	S_{21}	S_{23}	S_{32}	S_{31}
p_{11}	✓	✓	✓	✓	✓	✓	✓	✓	✓	✓
p_{22}	✓	✓	✓	✓	✓	✓	✓	✓	✓	✓
p_{33}	✓	✓	✓	✓	✓	✓	✓	✓	✓	✓
s_{31}	✓	$\times^*$	$\times^*$	×	✓	✓	×	×	×	×
s_{21}	✓	$\times^*$	$\times^*$	×	✓	✓	×	×	×	×
s_{12}	$\times^*$	✓	$\times^*$	×	×	×	✓	✓	×	×
s_{32}	$\times^*$	✓	$\times^*$	×	×	×	✓	✓	×	×
s_{23}	$\times^*$	$\times^*$	✓	×	×	×	×	×	✓	✓
s_{13}	$\times^*$	$\times^*$	✓	×	×	×	×	×	✓	✓

Table 1 shows that, in the L-L model, the probe will be sensitive to perturbations caused by the pump wave for all pump/probe cases.

4.3. Wave speeds: neo-Hookean model 1

For the strain-energy function (11) from (12), we obtain in component form

$$\frac{\partial W}{\partial F_{i\alpha}} = \mu F_{i\alpha} + (\lambda \ln \sqrt{I_3} - \mu) F^{-T}_{i\alpha}.$$

The second derivative of the strain-energy function is

$$\frac{\partial^2 W}{\partial F_{i\alpha} \partial F_{k\beta}} = \mu \delta_{ik} \delta_{\alpha\beta} + \lambda F^{-T}_{k\beta} F^{-T}_{i\alpha} - (\lambda \ln \sqrt{I_3} - \mu) F^{-1}_{\alpha k} F^{-1}_{\beta i},$$

where we have used

$$\frac{\partial (F^{-T})_{i\alpha}}{\partial F_{k\beta}} = -F^{-1}_{\alpha k} F^{-1}_{\beta i}.$$

Thus, using (24), the final result for elasticity tensor is

$$J\mathcal{A}_{0jilk} = \mu B_{jl}\delta_{ik} + \lambda \delta_{ji}\delta_{lk} + (\mu - \lambda \ln \sqrt{I_3})\delta_{jk}\delta_{li}. \tag{28}$$

This means that for P-wave probes, from (28) and (23), we obtain in compact form

$$\rho_0 v_{ii}^2 = J\mathcal{A}_{0iiii} = \mu B_{ii} + \lambda - \lambda \ln \sqrt{I_3} + \mu, \tag{29}$$

where v_{ii} is the velocity of a P-wave probe traveling along, and hence polarized along, X_i. (The i indices in the rest of the equation indicate the components of those tensors; no summation for i is implied here).

From expression (29), we see that P-wave probes will always depend on volumetric deformations through the invariant I_3, and therefore will always be perturbed by a P-wave pump (see table 1). However, there are only some cases when a P-wave probe will be affected by an S-wave pump. To show this, consider deformation gradients that correspond to a large underlying shear wave and calculate the corresponding left Cauchy-Green deformations tensors. There are six cases of shear deformation:

$$[\mathbf{F}_1] = \begin{bmatrix} 1 & \gamma & 0 \\ 0 & 1 & 0 \\ 0 & 0 & 1 \end{bmatrix}, \qquad [\mathbf{B}_1] = \begin{bmatrix} 1+\gamma^2 & \gamma & 0 \\ \gamma & 1 & 0 \\ 0 & 0 & 1 \end{bmatrix}, \tag{30}$$

$$[\mathbf{F}_2] = \begin{bmatrix} 1 & 0 & \gamma \\ 0 & 1 & 0 \\ 0 & 0 & 1 \end{bmatrix}, \qquad [\mathbf{B}_2] = \begin{bmatrix} 1+\gamma^2 & 0 & \gamma \\ 0 & 1 & 0 \\ \gamma & 0 & 1 \end{bmatrix}, \tag{31}$$

$$[\mathbf{F}_3] = \begin{bmatrix} 1 & 0 & 0 \\ \gamma & 1 & 0 \\ 0 & 0 & 1 \end{bmatrix}, \qquad [\mathbf{B}_3] = \begin{bmatrix} 1 & \gamma & 0 \\ \gamma & \gamma^2+1 & 0 \\ 0 & 0 & 1 \end{bmatrix}, \tag{32}$$

$$[\mathbf{F}_4] = \begin{bmatrix} 1 & 0 & 0 \\ 0 & 1 & \gamma \\ 0 & 0 & 1 \end{bmatrix}, \qquad [\mathbf{B}_4] = \begin{bmatrix} 1 & 0 & 0 \\ 0 & \gamma^2+1 & \gamma \\ 0 & \gamma & 1 \end{bmatrix}, \tag{33}$$

$$[\mathbf{F}_5] = \begin{bmatrix} 1 & 0 & 0 \\ 0 & 1 & 0 \\ 0 & \gamma & 1 \end{bmatrix}, \qquad [\mathbf{B}_5] = \begin{bmatrix} 1 & 0 & 0 \\ 0 & 1 & \gamma \\ 0 & \gamma & 1+\gamma^2 \end{bmatrix}, \tag{34}$$

$$[\mathbf{F}_6] = \begin{bmatrix} 1 & 0 & 0 \\ 0 & 1 & 0 \\ \gamma & 0 & 1 \end{bmatrix}, \qquad [\mathbf{B}_6] = \begin{bmatrix} 1 & 0 & \gamma \\ 0 & 1 & 0 \\ \gamma & 0 & \gamma^2+1 \end{bmatrix}, \tag{35}$$

where for simplicity we denote amount of shear by $\gamma = \partial u_i/\partial X_j$.

By noting the position of γ, we can quickly determine which probe waves will be influenced by a P-wave probe. There will be an effect on the P-wave probe when the propagation direction of the probe aligns with the polarization direction of the S-wave pump. (For example, for a probe travelling in the X_1-direction, (30) and (31), the amount of shear γ will influence the speed of a P-wave probe according to formula (29) for the P-wave probe, because of the dependence of B_{11} on γ. Note the positions of γ in the matrix expressions (30) and (31) of deformations gradients corresponding to shear deformations. This means that influencing shear wave pumps will be the waves, propagating in the X_2 direction and polarized in X_1 direction, and propagating in the X_3 direction with polarization in X_1 direction). We record the obtained results in table 1.

Note that here although simple shear deformation implies that each deformation gradient is such that $J = 1$, P-wave probe waves are in some cases influenced by the shear waves, which may seem counterintuitive. It is pertinent to mention analogous counterintuitive situation in non-linear elasticity for a stress-strain relationship, when simple shear deformation leads to diagonal components of stress and thus, unlike in the case of linear elasticity, the stress is not purely deviatoric, but also includes a pressure component. This is known as Kelvin effect in non-linear elasticity [23, 24].

Summarising we see that for the model (11) P-wave probes will always depend on volumetric deformations through invariant I_3, and therefore on P-wave pump, and in some cases, depending on their mutual orientation, P-wave probes will be also affected by shear wave pumps.

By examining (28) and (23) for shear wave probes we obtain 6 cases, which are expressed in terms of the components of the left Cauchy-Green deformation tensor.

For shear wave probes propagating in X_1 and polarized in X_3 direction and shear wave probes propagating in X_1 and polarized in X_2 direction, we obtain

$$\rho_0 v_{31}^2 = J\mathcal{A}_{01313} = \rho_0 v_{21}^2 = J\mathcal{A}_{01212} = \mu B_{11}. \tag{36}$$

For shear wave probes propagating in X_2 and polarized in X_1 direction and shear wave probes propagating in X_2 and polarized in X_3 direction, we obtain

$$\rho_0 v_{12}^2 = J\mathcal{A}_{02121} = \rho_0 v_{32}^2 = J\mathcal{A}_{02323} = \mu B_{22}. \tag{37}$$

For shear wave probes propagating in X_3 and polarized in X_2 direction and shear wave probes propagating in X_3 and polarized in X_1 direction, we obtain

$$\rho_0 v_{23}^2 = J\mathcal{A}_{03232} = \rho_0 v_{13}^2 = J\mathcal{A}_{03131} = \mu B_{33}. \tag{38}$$

The key observation from (36), (37), (38) and (30)–(35) is that in order for a probe wave to sense the pump, propagation direction of a S-wave probe should coincide with the polarization direction of the S-wave pump. We record the obtained results in table 1.

4.4. Wave speeds: neo-Hookean model 2 (decoupled energies)

From (15), the first derivative (first Piola-Kirchhoff stress tensor) in component form is

$$\frac{\partial W}{\partial F_{i\alpha}} = \mu I_3^{-1/3}\left(-\frac{1}{3}I_1 F_{i\alpha}^{-T} + F_{i\alpha}\right) + k(I_3 - \sqrt{I_3})F_{i\alpha}^{-T}. \tag{39}$$

Using (39), the second derivative is

$$\begin{aligned}\frac{\partial^2 W}{\partial F_{i\alpha}\partial F_{k\beta}} &= \mu\left(-\frac{2}{3}\right)I_3^{-1/3}F_{k\beta}^{-T}\left(-\frac{1}{3}F_{i\alpha}^{-T} + F_{i\alpha}\right)\\ &+\mu I_3^{-\frac{1}{3}}\left(-\frac{2}{3}F_{k\beta}F_{i\alpha}^{-T} + \frac{2}{3}I_1 F_{\alpha k}^{-1}F_{\beta i}^{-1} + \delta_{ik}\delta_{\alpha\beta}\right)\\ &+k(2I_3 F_{k\beta}^{-T} - \sqrt{I_3}F_{k\beta}^{-T})F_{i\alpha}^{-T} - k(I_3 - \sqrt{I_3})F_{\alpha k}^{-1}F_{\beta i}^{-1}.\end{aligned}$$

Using (24), the elasticity tensor is

$$\begin{aligned}J\mathcal{A}_{0jilk} &= \mu\left(-\frac{2}{3}\right)I_3^{-\frac{1}{3}}\delta_{lk}\left(-\frac{1}{3}I_1\delta_{ji} + B_{ji}\right)\\ &+ \mu I_3^{-\frac{1}{3}}\left(-\frac{2}{3}B_{kl}\delta_{ij} + \frac{1}{3}I_1\delta_{jk}\delta_{li} + B_{jl}\delta_{ik}\right)\\ &+ k(2I_3\delta_{lk} - \sqrt{I_3}\delta_{lk})\delta_{ji} - k(I_3 - \sqrt{I_3})\delta_{jk}\delta_{li}.\end{aligned} \tag{40}$$

For P-wave probes, from (40) and (23), in compact form

$$\rho_0 v_{ii}^2 = J\mathcal{A}_{0iiii} = \mu I_3^{-\frac{1}{3}}\left(\frac{5}{9}I_1 - \frac{1}{3}B_{ii}\right) + kI_3, \tag{41}$$

where v_{ii} is the P-wave probe velocity in direction X_i. (As above, the i indices in the rest of the equation indicate the components of respective tensors; no summation for i is implied).

Overall, P-wave probes will always be influenced by S-wave pumps through the invariant I_1, and influenced by P-wave pumps through the invariant I_3 (see table 1). We can also recover the classical expression in the reference configuration from (41) by recalling that bulk modulus $k = \frac{2}{3}\mu + \lambda$, to obtain $\rho_0 v_p^2 = \lambda + 2\mu$.

By examining (40) and (23) for shear wave probes we obtain 6 cases, which are expressed in terms of components of left Cauchy-Green deformation tensor.

For shear wave probes propagating in X_1, we obtain

$$\rho_0 v_{31}^2 = J\mathcal{A}_{01313} = \rho_0 v_{21}^2 = J\mathcal{A}_{01212} = \mu I_3^{-\frac{1}{3}} B_{11}. \tag{42}$$

For shear wave probes propagating in X_2, we obtain

$$\rho_0 v_{12}^2 = J\mathcal{A}_{02121} = \rho_0 v_{32}^2 = J\mathcal{A}_{02323} = \mu I_3^{-\frac{1}{3}} B_{22}. \tag{43}$$

For shear wave probes propagating in X_3, we obtain

$$\rho_0 v_{23}^2 = J\mathcal{A}_{03232} = \rho_0 v_{13}^2 = J\mathcal{A}_{03131} = \mu I_3^{-\frac{1}{3}} B_{33}. \tag{44}$$

Analyzing the obtained results (42), (43), (44) for S-wave probes and using (30)–(35), we conclude that the probe will sense the pump if the propagation direction of the probe aligns with the polarization direction of the pump.

Note it can be shown that

$$\bar{\mathbf{B}} = I_3^{-\frac{1}{3}}\mathbf{B}.$$

Therefore, the speeds of shear probe waves (42), (43), (44) will not depend on dilation/compression or, equivalently, a spherical P-wave, which is indicated in table 1.

5. Calculations for an example configuration

To demonstrate calculations of probe wave speed changes, we use an example configuration shown in figure 1 based on experimental work by [15], in which they applied a static load and a pump wave. Pump shear wave transducers (the source and the receiver) are attached to the X_2X_3 plane. Probe P- and S-wave transducers (the sources and the receivers) are attached to the X_1X_3 plane. A static load, such as applied by a press machine, acts along X_3.

5.1. Calculations: L-L model

The total deformation gradient is

$$\mathbf{F} = \mathbf{F}_2\mathbf{F}_1,$$

where $\mathbf{F}_1$ corresponds to a static deformation due to the applied load and $\mathbf{F}_2$ is the dynamic deformation corresponding to the pump wave. In matrix form,

$$[\mathbf{F}_1] = \begin{bmatrix} \lambda_1 & 0 & 0 \\ 0 & \lambda_2 & 0 \\ 0 & 0 & \lambda_3 \end{bmatrix}, \tag{45}$$

where $\lambda_1, \lambda_2, \lambda_3$ are (principal) stretches in the directions X_1, X_2, X_3, and

$$[\mathbf{F}_2] = \begin{bmatrix} 1 & 0 & 0 \\ \dfrac{\partial U_2}{\partial x_1} & 1 & 0 \\ 0 & 0 & 1 \end{bmatrix}, \tag{46}$$

where U_2 is the displacement induced by the pump wave. Therefore, the total deformation gradient is

$$[\mathbf{F}] = \begin{bmatrix} \lambda_1 & 0 & 0 \\ \lambda_1\dfrac{\partial U_2}{\partial x_1} & \lambda_2 & 0 \\ 0 & 0 & \lambda_3 \end{bmatrix}. \tag{47}$$

A matrix expression of the Green strain tensor (3) is

$$[\mathbf{E}] = \frac{1}{2}\begin{bmatrix} \lambda_1^2 + \left(\dfrac{\partial U_2}{\partial x_1}\right)^2\lambda_1^2 - 1 & \lambda_1\lambda_2\dfrac{\partial U_2}{\partial x_1} & 0 \\ \lambda_1\lambda_2\dfrac{\partial U_2}{\partial x_1} & \lambda_2^2 - 1 & 0 \\ 0 & 0 & \lambda_3^2 - 1 \end{bmatrix}. \tag{48}$$

From (47), we also obtain a matrix expression for the left Cauchy-Green deformation tensor

$$[\mathbf{B}] = \begin{bmatrix} \lambda_1^2 & \lambda_1^2\dfrac{\partial U_2}{\partial x_1} & 0 \\ \lambda_1^2\dfrac{\partial U_2}{\partial x_1} & \lambda_1^2\left(\dfrac{\partial U_2}{\partial x_1}\right)^2 + \lambda_2^2 & 0 \\ 0 & 0 & \lambda_3^2 \end{bmatrix}. \tag{49}$$

The Eulerian tensor $\mathbf{M}$ has components

$$[\mathbf{M}] = \begin{bmatrix} M_{11} & M_{12} & 0 \\ M_{21} & M_{22} & 0 \\ 0 & 0 & M_{33} \end{bmatrix}, \tag{50}$$

where

$$M_{11} = \frac{1}{2}\lambda_1^2\left(\lambda_1^2 + \frac{\partial U_2}{\partial x_1}\lambda_1^2 - 1\right),$$

$$M_{12} = M_{21} = \frac{1}{2}\lambda_1^2\frac{\partial U_2}{\partial x_1}\left(\lambda_1^2 + \left(\frac{\partial U_2}{\partial x_1}\right)^2\lambda_1^2 - 1\right) + \frac{1}{2}\lambda_1^2\lambda_2^2\frac{\partial U_2}{\partial x_1},$$

$$M_{22} = \frac{1}{2}\lambda_1^2\left(\frac{\partial U_2}{\partial x_1}\right)^2\left(\lambda_1^2 + \left(\frac{\partial U_2}{\partial x_1}\right)^2\lambda_1^2 - 1\right) + \lambda_1^2\lambda_2^2\left(\frac{\partial U_2}{\partial x_1}\right)^2 + \frac{1}{2}\lambda_2^2(\lambda_2^2 - 1),$$

$$M_{33} = \frac{1}{2}\lambda_3^2(\lambda_3^2 - 1).$$

Our example considers a P-wave probe travelling (and polarized) along X_2. Thus, both vectors **m** and **n** will have components (0, 1, 0). Thus, we find from (23) that for a P-wave probe

$$\rho_0 v_{22}^2 = J\mathcal{A}_{02222}. \tag{51}$$

For an S-wave probe that propagates along X_2 with polarization along X_3, the unit vectors **n** and **m** have components (0, 1, 0) and (0, 0, 1), respectively. Applied to (23), this gives

$$\rho_0 v_{32}^2 = J\mathcal{A}_{02323}. \tag{52}$$

To show the wave speed corresponding to the model (4), we use (51) and (25) to express the P-wave probe speed as

$$\begin{aligned}\rho_0 v_{22}^2 = {} & (\lambda + 2\mu + 2CI_1 + 2FI_2 + 12HI_1^2 + 2BI_1 + 2FI_1^2 \\ & + 4GI_2)B_{22}B_{22} + (2A + 6AI_1 + 4B + 6E \\ & + 8FI_1)B_{22}M_{22} + 8GM_{22}M_{22} + (\lambda I_1 + BI_2 + CI_1^2 \\ & + EI_3 + 2FI_1I_2 + 4HI_1^3)B_{22} \\ & + 2M_{22}(\mu + BI_1 + FI_1^2 + 2GI_2) + \bar{M}_{22}.\end{aligned} \tag{53}$$

We note that, in the reference configuration where predeformation reduces to the identity tensor and the strain tensor reduces to the zero strain tensor, we recover classical result for P-waves $\rho v_p^2 = \lambda + 2\mu$. Similarly, from (52) and (25) for the underlying deformation (47), the S-wave probe speed is

$$\begin{aligned}\rho_0 v_{32}^2 = {} & (\mu + BI_1 + FI_1^2 + 2GI_2)B_{22}B_{33} \\ & + (\lambda I_1 + BI_2 + CI_1^2 + EI_3 + 2FI_1I_2 + 4HI_1^3)B_{22} \\ & + 2M_{22}(\mu + BI_1 + FI_1^2 + 2GI_2) + \bar{M}_{22}.\end{aligned} \tag{54}$$

The expressions for invariants I_1, I_2 and I_3 are quite lengthy, so they are shown in appendix C.

To demonstrate that the above expressions are physically reasonable, figure 2 compares the phase speeds of probe waves (either P or S) when they are perturbed by both a dynamic pump (S-wave) and a static load.

For context, we model the solid with parameters that are appropriate for Crab Orchard sandstone (from [26]: mass density $\rho = 2285$ kg m^{-3}, $\mu = 7.6$ GPa, $\lambda = 4.6$ GPa, $A = -3.49 \cdot 10^4$ GPa, $B = -4.705 \cdot 10^4$ GPa, $C = -2.695 \cdot 10^4$ GPa). Since there is no data available for fourth-order material constants, we use L-L model up to the third-order of expansion. We model the displacement caused by a sinusoidal S-wave pump

$$U_2 = A\sin(kx_1 - \omega t),$$

where A is the amplitude ($3.83 \cdot 10^{-9}$ m), k is wave number (261 m^{-1}) and ω is the angular frequency of the pump wave ($2\pi \cdot 90$ kHz). The required derivative in (47) is

$$\frac{\partial U_2}{\partial x_1} = Ak\cos(kx_1 - \omega t).$$

The deformation caused by the static load induces a sample stretch λ_3, so figure 2 shows how the probe wave speed changes with sample stretch due to the static deformation. In the experimental setup (figure 1), the lateral sides of the sample are not constrained, therefore the sample will be deformed in the directions perpendicular to the vertical load. Thus, our calculations assume that vertical and stretches along X_1 and X_2 directions are connected by the approximate formula $\lambda_1 = \lambda_2 = \sqrt{1 - 0.19(\lambda_3^2 - 1)}$, which follows from Biot definition of Poisson's ratio for finite strains with $\nu = 0.19$. Figure 2 shows that our calculations yield faster probe speeds under compressive static load ($\lambda < 1$) and slower under tensile load ($\lambda > 1$), and P-waves probes travel faster than S-wave probes; both of these trends are expected. What is harder to see on the scale of the figure is that there

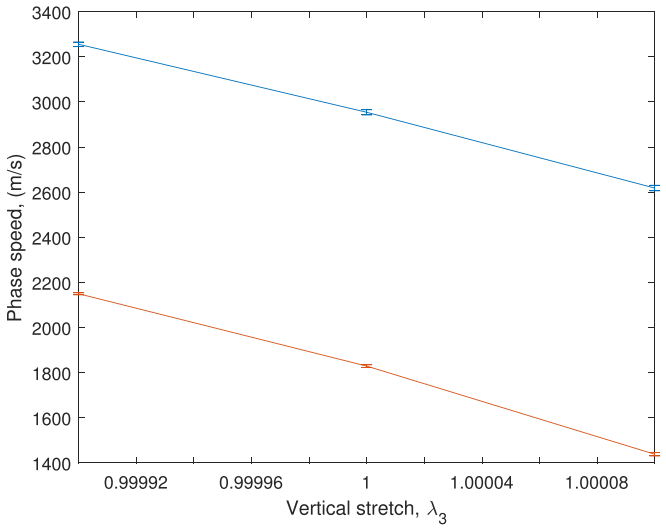

Figure 2. Calculation of phase speed variation for probe waves (P-wave (blue) and S-wave (red)) when perturbed by both a dynamic (sinusoidal) S-wave pump and a static pre-deformation λ, using the L-L model.

are also small variations in phase speed due to the dynamic pump (~10 m s^{-1}, which is contained within the dimensions of the plot markers). We see that the range of variation due to the pump wave not independent of the predeformation: compressive loads cause less variation in the pump-induced perturbation relative to tensile loads.

5.2. Calculations: neo-Hookean model 1

For neo-Hookean model 1 in (11), P-wave probes with equation (29) yield

$$\rho_0 v_{22}^2 = J\mathcal{A}_{02222} = \mu B_{22} + \lambda - \lambda \ln \sqrt{I_3} + \mu,$$

where from (49)

$$B_{22} = \lambda_1^2\left(\frac{\partial U_2}{\partial x_1}\right)^2 + \lambda_2^2, \tag{55}$$

and also

$$I_3 = \det\mathbf{C} = \det\mathbf{B} = \lambda_1^4\lambda_3^2\left(\frac{\partial U_2}{\partial x_1}\right)^2 + \lambda_1^2\lambda_2^2\lambda_3^2 - \lambda_1^4\lambda_3^2\left(\frac{\partial U_2}{\partial x_1}\right)^2. \tag{56}$$

Analogously, the speed of a S-wave probe is

$$\rho_0 v_{32}^2 = J\mathcal{A}_{02323} = \mu B_{22} = \mu\left[\lambda_1^2\left(\frac{\partial U_2}{\partial x_1}\right)^2 + \lambda_2^2\right].$$

5.3. Calculations: neo-Hookean model 2 (decoupled energies)

Using expression (41), the P-wave probe speeds are

$$\rho_0 v_{22}^2 = J\mathcal{A}_{02222} = \mu I_3^{-\frac{1}{3}}\left(\frac{5}{9}I_1 - \frac{1}{3}B_{22}\right) + kI_3,$$

where $I_1 = \mathrm{tr}\mathbf{C} = \mathrm{tr}\mathbf{B} = \lambda_1^2 + \lambda_1^2\left(\frac{\partial U_2}{\partial x_1}\right)^2 + \lambda_2^2 + \lambda_3^2$.

Similarly, (43) gives S-wave probe speeds

$$\rho_0 v_s^2 = J\mathcal{A}_{02323} = \mu I_3^{-\frac{1}{3}} B_{22}.$$

The other required expressions B_{22} and I_3 are the same as in section 5.2 and given by expressions (55) and (56).

Results for neo-Hookean models (11) and (14) are qualitatively similar to results above, so we do not show them here. The main difference between all neo-Hookean models and the L-L model is that the neo-Hookean models appear to be much less sensitive, in that the dynamic perturbations caused by the pump wave are so small that they can be neglected.

6. Discussion

Our results present detailed and systematic theoretical underpinnings for static and dynamic acoustoelastic testing for isotropic non-linear elastic materials. This is particularly relevant for dynamic acoustoelastic effects in pump-probe experiments, since we find that the ways in which pump waves are predicted to perturb a probe wave depend on the choice of model. Below, we discuss where gaps still exist in linking models with experiments, and show how the present work begins to address such gaps.

The primary challenge with modelling dynamic acoustoelasticity is that, in order to apply a theory in a tractable manner, it is necessary to make assumptions about the nature of the material as well as the nature of the waves. It is not always feasible to determine whether such assumptions are valid in a given experimental situation.

For example, [27] is one of the first to use dynamic acoustoelastic testing to determine a full set of third-order elastic constants (l, m and n). While their experiments were dynamic, the theoretical analyses involved a third-order model [28] that was previously used for static acoustoelastic testing, which requires an assumption that the underlying strain field traversed by the probe wave is homogeneous and static. In another case [5], wave speeds were derived in terms of principle stretches, which is a scenario that would be suitable for samples under hydrostatic pressure and/or uniaxial, biaxial or triaxial tests, but not appropriate for shear wave deformations [8]. In principle, shear deformation can be expressed in terms of principal stretches along the Lagrangian or Eulerian principal axes [24]. However, if the levels of shear deformation change, then principal axes also change, making the theoretical approach used in [5] very difficult to execute in practice. Thus, it is very challenging to design an experiment that rigorously satisfies all the assumptions of a given model.

There is great potential for development of models required for static and dynamic acoustoelastic testing. For example, the L-L model, which is an expression of a strain-energy function up to the third-order of non-linearity in the strain $\mathbf{E}$, was first sketched in different notation in Volume 7 (p. 107) of a very popular general course of physics [21] with no detailed analysis. Nonetheless, this model became a default model in many acoustoelastic studies. Here, we present useful developments by extending this model to the fourth-order in $\mathbf{E}$, and providing a full expression of the elasticity tensor (25) as well as full expressions for P-wave and S-wave probe speeds associated with this model for any underlying deformation, including shear deformation.

In developing further the L-L model, we also uncovered a conceptual flaw in it. In more traditional non-linear elastic models [23], volumetric deformations are captured by introducing $\det\mathbf{C}$ in the strain-energy function, since its physical meaning is the square of the volume ratio between the current and reference configurations $(dv/dV)^2$. However, the L-L model uses traces of strain $\mathbf{E}$, so it is not clear how pure volumetric deformations are captured. This leads to a troubling consequence that calculation of stress using expression (10) for simple shear leads to an expression in which the stress depends on Lamé's parameter λ, which is a measure of how easily a material can undergo volumetric deformations. Since simple shear does not change volumetric deformation, the presence of Lamé's parameter λ here cannot be justified. Similarly, our calculations show that the L-L model leads to S-wave probe speeds that depend on the linear elastic parameter λ (such as in (27)). More details of our calculations on these troubling consequences and some remarks on parameter λ within the context of linear and nonlinear elasticity are given in appendix A.

Given the limitations of the L-L model, we also considered two neo-Hookean models. In the first version described in (11), the second and the third terms clearly depend on invariant $I_3 = \det\mathbf{C}$, and thus they have a clear physical meaning. Note that the first term in (11), as a function of invariant I_1, depends both on distortional isochoric and dilatational deformations. In the second version described in (14), the energies due to distortional and dilatational deformations are fully decoupled. Note that the first term in (14) activates only if we have distortional deformation and the second term activates only if volumetric deformations are present.

As a way to compare all three models, table 1 summarizes when a certain type of probe wave will have a speed that is perturbed by a given pump wave type. Even though all three models are isotropic, the static and dynamic deformations cause differences in when shifts in probe wave speeds occur. In the L-L model, any probe wave will be perturbed by any type of pump. However, this is not the case for the two neo-Hookean models, and there are consequences for the energy splitting with respect to which probe waves feel which pump wave perturbations. For example, in the decoupled model (version 2), spherical P-waves pumps have no impact on S-wave probes and P-wave probes will be perturbed by all P- and S-wave pumps, which is different from the coupled model (version 1).

It is worth describing the different results of each model in broad terms, focusing on the probe wave speed perturbations that are central to our study. Since shear waves do not change volume, we may intuitively think that S-wave pumps are not supposed to influence P-wave probes, (which should sense on pressure

changes in the material). Table 1 shows that this is not universally true in our models. For example, all P-wave probes are perturbed by any P-wave pump, as expected. However, our results show that large amplitude S-waves (while still being volume preserving) may still influence P-waves (compare the first three lines in table 1 for model (11)). To explain this, we point to the Kelvin effect, which appears only in nonlinear elasticity [23, 24]: for a simple shear deformation, linear elasticity does not yield diagonal components in the stress tensor, but it does yield such diagonal elements in non-linear elasticity.

Now, let us consider the case when P-waves represent pumps and S-waves represent probes. In this case, P-wave pumps will influence the S-wave probes only if polarization direction and propagation direction of P-wave pumps coincides with the propagation direction (propagation direction corresponds to the second index) of S-wave probes. Physically, this can be explained in the following way. Imagine that an S-wave probe (with polarization normal to polarization of P-wave pump) propagates in the region of compression (or rarefaction) caused by the P-wave pump. In a transverse wave the source excites neighbouring molecules in the direction perpendicular to the propagation direction of the wave, in turn these molecules due to intermolecular forces pull other neighboring molecules causing oscillation of the neighboring region of molecules and this process continues, and thus the transverse wave propagates. In the region of compression (or rarefaction), the P-wave pump changes the forces by means of which the neighboring molecules interact. This leads to changes in the time of interaction between the neighboring molecules and hence we expect that S-wave probe will propagate with a different speed. Finally, consider the case of S-wave pumps and S-wave probes. From table 1 we observe that the S-wave pump will influence the S-wave probe in cases when polarization direction of the pump wave (S-wave) coincide with the propagation direction of probe wave (S-wave). Using similar arguments as those used for P-wave pump and S-wave probe, the action of the S-wave pump on the S-wave probe can be explained.

Finally, even though we have highlighted the relevance of our models for dynamic deformations, it is important to emphasize that our derivations apply equally well to static deformations. Static deformation has relevance for dynamic pump-probe experiments under field conditions, since earth solids are often deformed due to gravitational forces. Similarly, the compressive load of large masses of water are important to consider at depth in oceans. Accounting for predeformation/prestress in these situations could have a significant effect in models designed to calculate propagation speeds of probe waves.

7. Conclusions

In this paper, we considered three non-linear isotropic models for acoustoelasticity. Our derivations relied on the context of modern continuum mechanics, based on a theory of small deformations superimposed on large deformations [24], and yielded elasticity tensors and propagation speeds of P- and S-wave probes. Our results are general and can be applied to different types of underlying deformations and probe waves, including different polarizations and propagation directions. In doing this, we found that whether a specific probe wave will be sensitive to another specific pump wave will depend on the material model. Furthermore, it is evident that the results for P- and S-wave probes are different even though all considered material models were isotropic, non-linear elastic models. Also, we have concluded that usage of L-L model leads to an inconsistent result, namely that simple shear deformation induces a stress that depends on the Lamé parameter λ and shear wave probes also depend on λ, which is inconsistent with the definition of λ related to resistance to volumetric deformations.

Acknowledgments

Funding is acknowledged from Natural Sciences and Engineering Research Council (NSERC) Canada through grants IRCPJ 491 051-14 and 2018-04888, as well as from Chevron and InnovateNL.

Data availability statement

All data that support the findings of this study are included within the article (and any supplementary files).

Appendix A. Stress calculation for simple shear deformation for Landau–Lifshitz model and some remarks about parameter λ

Let us consider isochoric distortional deformation (simple shear)

$$[\mathbf{F}] = \begin{bmatrix} 1 & \gamma & 0 \\ 0 & 1 & 0 \\ 0 & 0 & 1 \end{bmatrix},$$

where $\gamma = \frac{\partial u_1}{\partial X_2}$ is the amount of shear. The considered deformation does not change volume, as confirmed by

$$\det\mathbf{F} = 1. \tag{A.1}$$

The Green (Lagrangian) strain tensor can be obtained from expression (3). The non-zero components of Green (Lagrangian) strain tensor are

$$[\mathbf{E}] = \begin{bmatrix} 0 & E_{12} & 0 \\ E_{21} & E_{22} & 0 \\ 0 & 0 & 0 \end{bmatrix},$$

where $E_{12} = E_{21} = \frac{1}{2}\gamma$, $E_{22} = \frac{1}{2}\gamma^2$.

The required expression for squared $\mathbf{E}$ is

$$[\mathbf{E}^2] = \begin{bmatrix} E_{12}^2 & E_{12}E_{22} & 0 \\ E_{22}E_{21} & E_{12}^2 + E_{22}^2 & 0 \\ 0 & 0 & 0 \end{bmatrix}.$$

We calculate the required invariants

$$I_1 = \frac{1}{2}\gamma^2, \quad I_2 = \frac{1}{4}(2\gamma^2 + \gamma^4), \quad I_3 = \frac{1}{8}(3\gamma^4 + \gamma^6),$$
$$I_1^2 = \frac{1}{4}\gamma^4, \quad I_1^3 = \frac{1}{6}\gamma^6, \quad I_1 I_2 = \frac{1}{8}(2\gamma^4 + \gamma^6).$$

Substituting the preceding expressions into (10), we obtain the components of the second Piola-Kirchhoff stress tensor

$$\begin{aligned} S_{11} &= \frac{\lambda}{2}\gamma^2 + \frac{B}{4}(2\gamma^2 + \gamma^4) + \frac{C}{4}\gamma^4 + \frac{E}{8}(3\gamma^4 + \gamma^6) \\ &\quad + \frac{F}{4}(2\gamma^4 + \gamma^6) + \frac{H}{2}\gamma^6 + (A + \frac{3}{2}E\gamma^2)\frac{\gamma^2}{4}, \\ S_{12} = S_{21} &= (\mu + \frac{B}{2}\gamma^2 + \frac{F}{4}\gamma^4 + \frac{G}{2}(2\gamma^2 + \gamma^4))\gamma \\ &\quad + (A + \frac{3}{2}E\gamma^2)\frac{\gamma^3}{4}, \\ S_{22} &= \frac{\lambda}{2}\gamma^2 + \frac{B}{4}(2\gamma^2 + \gamma^4) + \frac{C}{4}\gamma^4 + \frac{E}{8}(3\gamma^4 + \gamma^6) \\ &\quad + \frac{F}{4}(2\gamma^4 + \gamma^6) + \frac{H}{2}\gamma^6 \\ &\quad + (\mu + \frac{B}{2}\gamma^2 + \frac{F}{4}\gamma^4 + \frac{G}{2}(2\gamma^2 + \gamma^4))\gamma^2 \\ &\quad + (A + \frac{3}{2}E\gamma^2)\frac{\gamma^2}{4}, \\ S_{33} &= \frac{\lambda}{2}\gamma^2 + \frac{B}{4}(2\gamma^2 + \gamma^4) + \frac{C}{4}\gamma^4 + \frac{E}{8}(3\gamma^4 + \gamma^6) \\ &\quad + \frac{F}{4}(2\gamma^4 + \gamma^6) + \frac{H}{2}\gamma^6. \end{aligned}$$

We see that despite the fact that we are dealing with a volume preserving deformation, λ is present in the expressions of components S_{11}, S_{22}, S_{33} which cannot be justified physically.

Let us make several remarks about the physical meaning of λ in the context of linear and nonlinear elasticity. Since we can write the classical connection for parameter λ

$$\lambda = \kappa - \frac{2}{3}\mu, \tag{A.2}$$

where κ is the bulk modulus and $K = 1/\kappa$ is the compressibility, it is true that λ depends on both compressibility K and shear modulus μ. Nonetheless, we have to emphasise that compressibility K is only included in λ. Let us consider the expression for weighted stress in equation (13). According to the formula (13), for shear (isochoric) deformation, it makes sense that the resulting expression for stress will not include term with λ, because in this case $I_3 = 1$ and since bulk modulus κ is included only in λ according to (A.2), not in μ. For shear deformation μ comes from the term $\mu(\mathbf{B} - \mathbf{I})$ in formula (13) for the respective stress.

For comparison, in linear elastic case we have

$$\boldsymbol{\sigma} = \lambda(\mathrm{tr}\boldsymbol{\epsilon})\mathbf{I} + 2\mu\boldsymbol{\epsilon}. \tag{A.3}$$

Therefore, for shear isochoric deformation ($\mathrm{tr}\boldsymbol{\epsilon} = 0$) the resulting expression for stress has a term with μ (no term with λ). Thus, we note the physical consistency of model (11) with linear elastic case.

Furthermore, let us consider the term $\lambda \ln \sqrt{I_3}\mathbf{I}$ in expression (13). It makes sense that due to the large value of λ it is hard to change the volume, and because of that even small changes in volume (and thus in I_3) will result in high stress.

In summary, we note that λ is not fully decoupled from μ and it has a complicated physical meaning, nonetheless, we argue that for the overall physical consistency μ should appear in the expression for stress from other terms (not from the terms containing λ) when we are dealing with isochoric deformations.

Appendix B. Some details of derivation of elasticity tensor for fourth-order elasticity model

Using the chain rule

$$\frac{\partial W}{\partial F_{i\alpha}} = \frac{\partial W}{\partial E_{\theta\omega}}\frac{\partial E_{\theta\omega}}{\partial F_{i\alpha}}.$$

Using a product rule and a chain rule, we obtain

$$\frac{\partial^2 W}{\partial F_{i\alpha}\partial F_{k\beta}} = \frac{\partial^2 W}{\partial E_{\theta\omega}\partial E_{\gamma\tau}}\frac{\partial E_{\gamma\tau}}{\partial F_{k\beta}}\frac{\partial E_{\theta\omega}}{\partial F_{i\alpha}} + \frac{\partial W}{\partial E_{\theta\omega}}\frac{\partial}{\partial F_{k\beta}}\left(\frac{\partial E_{\theta\omega}}{\partial F_{i\alpha}}\right). \tag{B.1}$$

From (3) we obtain in index notation

$$E_{\theta\omega} = \frac{1}{2}(F_{m\theta}F_{m\omega} - \delta_{\theta\omega})$$

and thus

$$\frac{\partial E_{\theta\omega}}{\partial F_{i\alpha}} = \frac{1}{2}(F_{i\omega}\delta_{\theta\alpha} + F_{i\theta}\delta_{\omega\alpha}). \tag{B.2}$$

Also,

$$\frac{\partial E_{\gamma\tau}}{\partial F_{k\beta}} = \frac{1}{2}(F_{k\tau}\delta_{\gamma\beta} + F_{k\gamma}\delta_{\tau\beta}). \tag{B.3}$$

Therefore,

$$\frac{\partial}{\partial F_{k\beta}}\left(\frac{\partial E_{\theta\omega}}{\partial F_{i\alpha}}\right) = \frac{1}{2}(\delta_{ik}\delta_{\omega\beta}\delta_{\theta\alpha} + \delta_{ik}\delta_{\theta\beta}\delta_{\omega\alpha}). \tag{B.4}$$

Thus, substituting expressions (B.2), (B.3) and (B.4) in (B.1), after some rearrangements, we obtain

$$\frac{\partial^2 W}{\partial F_{i\alpha}\partial F_{k\beta}} = \frac{\partial^2 W}{\partial E_{\alpha\omega}\partial E_{\gamma\beta}}F_{k\gamma}F_{i\omega} + \frac{\partial W}{\partial E_{\alpha\beta}}\delta_{ik}.$$

Thus, from (24) we obtain

$$J\mathcal{A}_{0jilk} = F_{j\alpha}F_{l\beta}F_{k\gamma}F_{i\omega}\frac{\partial^2 W}{\partial E_{\alpha\omega}\partial E_{\gamma\beta}} + F_{j\alpha}F_{l\beta}\frac{\partial W}{\partial E_{\alpha\beta}}\delta_{ik}. \tag{B.5}$$

Using the strain energy function (4), we obtain

$$\begin{aligned}\frac{\partial W}{\partial E_{\alpha\omega}} &= (\lambda I_1 + BI_2 + CI_1^2 + EI_3 + 2FI_1I_2 + 4HI_1^3)\delta_{\alpha\omega} \\ &+ (\mu + BI_1 + FI_1^2 + 2GI_2)(E_{\alpha\omega} + E_{\omega\alpha}) \\ &+ (A + 3EI_1)(\mathbf{E}^2)_{\alpha\omega} \end{aligned} \tag{B.6}$$

and

$$\begin{aligned}\frac{\partial^2 W}{\partial E_{\alpha\omega}\partial E_{\gamma\beta}} &= (\lambda\delta_{\gamma\beta} + 2BE_{\gamma\beta} + 2CI_1\delta_{\gamma\beta} + 3E(\mathbf{E}^2)_{\gamma\beta} \\ &+2FI_2\delta_{\gamma\beta} + 4FI_1E_{\gamma\beta} + 12HI_1^2\delta_{\gamma\beta})\delta_{\alpha\omega} \\ &+(B_{\gamma\beta} + 2FI_1\delta_{\gamma\beta} + 4GE_{\gamma\beta})(E_{\alpha\omega} + E_{\omega\alpha}) \\ &+(\mu + BI_1 + FI_1^2 + 2GI_2)(\delta_{\alpha\gamma}\delta_{\omega\beta} + \delta_{\omega\gamma}\delta_{\alpha\beta}) \\ &+3E\delta_{\gamma\beta}(\mathbf{E}^2)_{\alpha\omega} + (A + 3EI_1)(\delta_{\alpha\gamma}E_{\beta\omega} + E_{\alpha\gamma}\delta_{\omega\beta}). \end{aligned} \tag{B.7}$$

Substituting (B.6) and (B.7) into (B.5), after some rearrangements, we obtain expression for elasticity tensor given in equation (25).

Appendix C. Calculation of invariants I_1, I_2, I_3

We calculate the invariants I_1, I_2 and I_3, required in expressions (53) and (54), for the specific deformation (47)

$$I_1 = 0.5\left(\lambda_1^2 + \lambda_2^2 + \lambda_3^2 - 3 + \left(\frac{\partial U_2}{\partial x_1}\right)\lambda_1^2\right),$$

$$\begin{aligned}I_2 = 0.25&\left(\lambda_1^2\left(\frac{\partial U_2}{\partial x_1}\right)^2 + \lambda_1^2 - 1\right)^2 + 0.25(\lambda_2 - 1)^2 \\ &+ 0.25(\lambda_3 - 1)^2 + 0.5\lambda_1^2\lambda_2^2\lambda_3^2\left(\frac{\partial U_2}{\partial x_1}\right)^2.\end{aligned}$$

Next quantities become quite cumbersome and complicated. In order to simplify notation we introduce in this section $\lambda_1 \equiv a$, $\lambda_2 \equiv b$, $\lambda_3 \equiv c$ and $\frac{\partial U_2}{\partial x_1} \equiv d$.

Thus, we obtain

$$\begin{aligned}I_3 = &(((a^2d^2)/2 + a^2/2 - 1/2)^2 + (a^2b^2d^2)/4)((a^2d^2)/2 \\ &+ a^2/2 - 1/2) + (b^2/2 - 1/2)((b^2/2 - 1/2)^2 \\ &+ (a^2b^2d^2)/4).\end{aligned}$$

We find that

$$\begin{aligned}I_1^2 = &(a^4 * d^4)/4 + (a^4 * d^2)/2 + a^4/4 + (a^2 * b^2 * d^2)/2 \\ &+ (a^2 * b^2)/2 + (a^2 * c^2 * d^2)/2 + (a^2 * c^2)/2 \\ &- (3 * a^2 * d^2)/2 - (3 * a^2)/2 + b^4/4 + (b^2 * c^2)/2 \\ &- (3 * b^2)/2 + c^4/4 - (3 * c^2)/2 + 9/4,\end{aligned}$$

$$\begin{aligned}I_1^3 = &(a^6 * d^6)/8 + (3 * a^6 * d^4)/8 + (3 * a^6 * d^2)/8 + a^6/8 \\ &+ (3 * a^4 * b^2 * d^4)/8 + (3 * a^4 * b^2 * d^2)/4 + (3 * a^4 * b^2)/8 \\ &+ (3 * a^4 * c^2 * d^4)/8 + (3 * a^4 * c^2 * d^2)/4 + (3 * a^4 * c^2)/8 \\ &- (9 * a^4 * d^4)/8 - (9 * a^4 * d^2)/4 - (9 * a^4)/8 \\ &+ (3 * a^2 * b^4 * d^2)/8 + (3 * a^2 * b^4)/8 \\ &+ (3 * a^2 * b^2 * c^2 * d^2)/4 + (3 * a^2 * b^2 * c^2)/4 \\ &- (9 * a^2 * b^2 * d^2)/4 - (9 * a^2 * b^2)/4 + (3 * a^2 * c^4 * d^2)/8 \\ &+ (3 * a^2 * c^4)/8 - (9 * a^2 * c^2 * d^2)/4 - (9 * a^2 * c^2)/4 \\ &+ (27 * a^2 * d^2)/8 + (27 * a^2)/8 + b^6/8 + (3 * b^4 * c^2)/8 \\ &- (9 * b^4)/8 + (3 * b^2 * c^4)/8 - (9 * b^2 * c^2)/4 + (27 * b^2)/8 \\ &+ c^6/8 - (9 * c^4)/8 + (27 * c^2)/8 - 27/8,\end{aligned}$$

$$I_1 I_2 = (((a^2 * d^2)/2 + a^2/2 - 1/2)^2 + (b^2/2 - 1/2)^2 + (c^2/2 - 1/2)^2 + (a^2 * b^2 * d^2)/2) * ((a^2 * d^2)/2 + a^2/2 + b^2/2 + c^2/2 - 3/2).$$

The complete matrix expression of $\bar{\mathbf{M}}$ is very long, therefore, we only give component $\bar{M}_{22}$, required in (53) and (54)

$$\bar{M}_{22} = b * ((b^2/2 - 1/2) * ((b * a^2 * d^2)/2 + b * (b^2/2 - 1/2)) + (a * b * d * ((a * d * b^2)/2 + a * d * ((a^2 * d^2)/2 + a^2/2 - 1/2)))/2) + a * d * (((a * d * b^2)/2 + a * d * ((a^2 * d^2)/2 + a^2/2 - 1/2)) * ((a^2 * d^2)/2 + a^2/2 - 1/2) + (a * b * d * ((b * a^2 * d^2)/2 + b * (b^2/2 - 1/2)))/2).$$

ORCID iDs

Andrey Melnikov https://orcid.org/0000-0001-8639-0000
Alison E Malcolm https://orcid.org/0000-0003-2775-7647
Kristin M Poduska https://orcid.org/0000-0003-4495-0668

References

[1] Gennisson J-L, Renier M, Catheline S, Barriere C, Bercoff J, Tanter M and Fink M 2007 Acoustoelasticity in soft solids: Assessment of the nonlinear shear modulus with the acoustic radiation force *The Journal of the Acoustical Society of America* **122** 3211–9
[2] Graham R A 1972 Determination of third- and fourth-order longitudinal elastic constants by shock compression techniques—application to sapphire and fused quartz *The Journal of the Acoustical Society of America* **51** 1576–81
[3] Lang J M and Gupta Y M 2011 Experimental determination of third-order elastic constants of diamond *Phys. Rev. Lett.* **106** 125502
[4] Yost W T and Breazeale M A 1973 Adiabatic third-order elastic constants of fused silica *J. Appl. Phys.* **44** 1909–10
[5] Abiza Z, Destrade M and Ogden R W 2012 Large acoustoelastic effect *Wave Motion* **49** 364–74
[6] Birch F 1938 The effect of pressure upon the elastic parameters of isotropic solids, according to murnaghan's theory of finite strain *J. Appl. Phys.* **9** 279–88
[7] Tang S 1967 Wave propagation in initially-stressed elastic solids *Acta Mech.* **9** 279–88
[8] Gallot T, Malcolm A, Szabo T L, Brown S, Burns D and Fehler M 2015 Characterizing the nonlinear interaction of s- and p-waves in a rock sample *J. Appl. Phys.* **117** 034902
[9] Renaud G, Callé S and Defontaine M 2009 Remote dynamic acoustoelastic testing: elastic and dissipative acoustic nonlinearities measured under hydrostatic tension and compression *Appl. Phys. Lett.* **94** 011905
[10] Rivière J, Renaud G, Guyer R A and Johnson P A 2013 Pump and probe waves in dynamic acousto-elasticity: Comprehensive description and comparison with nonlinear elastic theories *J. Appl. Phys.* **054905** 1–19
[11] Renaud G, Calle S, Remenieras J P and Defontaine M 2008 Exploration of trabecular bone nonlinear elasticity using time-of-flight modulation *IEEE Trans. Ultrason. Ferroelectr. Freq. Control* **55** 1497–507
[12] Renaud G, Le Bas P-Y and Johnson P A 2012 Revealing highly complex elastic nonlinear (anelastic) behavior of Earth materials applying a new probe: Dynamic acoustoelastic testing *J. Geophys. Res.* **117** B06202
[13] Renaud G, Riviere J, Larmat C, Rutledge J T, Lee R C, Guyer R A, Stokoe K and Johnson P 2014 In situ characterization of shallow elastic nonlinear parameters with Dynamic Acousto-Elastic Testing *J. Geophys. Res.* **109** 6907–23
[14] Guyer R A and Johnson P A 1999 Nonlinear mesoscopic elasticity: evidence for a new class of materials *Phys. Today* **52** 30–6
[15] Malcolm A, Hayes L, Moravej K, Melnikov A, Poduska K and Butt S 2021 Experimental monitoring of nonlinear wave interactions under uniaxial load *Earth and Space Science Open Archive* (https://doi.org/10.1002/essoar.10509364.1)
[16] Treloar L R G 1948 Stresses and birefringence in rubber subjected to general homogeneous strain *Proc. Phys. Soc* **60** 135
[17] Mooney M 1940 A theory of large elastic deformation *J. Appl. Phys.* **11** 582–92
[18] Gent A N and New A 1996 Constitutive Relation for Rubber *Rubber Chem. Technol.* **69** 59–61
[19] Arruda E M and Boyce M C 1993 A three-dimensional constitutive model for the large stretch behavior of rubber elastic materials *J. Mech. Phys. Solids* **41** 389–412
[20] Ogden R 1972 Large deformation isotropic elasticity—on the correlation of theory and experiment for incompressible rubberlike solids *Proc. R. Soc. Lond.* A **326** 565–84
[21] Landau L D and Lifshitz E M 1959 *Theory of Elasticity* ed J B Sykes and W H Reid (London: Pergamon)
[22] Johnson P A and Guyer R A 2009 *Nonlinear Mesoscopic Elasticity: The Complex Behaviour of Rocks, Soil, Concrete* (New York: Wiley)
[23] Bonet J and Wood R D 2008 *Nonlinear Continuum Mechanics for Finite Element Analysis* (Cambridge: Cambridge University Press)
[24] Ogden R W 1997 *Non-linear Elastic Deformations. Dover Civil and Mechanical Engineering* (Mineola, NY: Dover)
[25] Melnikov A and Ogden R W 2018 Bifurcation of finitely deformed thick-walled electroelastic cylindrical tubes subject to a radial electric field *Zeitschrift für angewandte Mathematik und Physik* **69** 60
[26] Rusmanugroho H, Malcolm A and Darijani M 2020 A numerical model for the nonlinear interaction of elastic waves with cracks *Wave Motion* **92** 102444
[27] Renaud G, Talmant M and Marrelec G 2016 Microstrain-level measurement of third-order elastic constants applying dynamic acousto-elastic testing *J. Appl. Phys.* **120** 135102
[28] Murnaghan F D 1951 *Finite Deformations of an Elastic Solid* (London: Chapman and Hall)